Classical Bouc-Wen hysteresis modeling and force control of a piezoelectric robotic hand manipulating deformable object
Supplementary material

Gerardo Flores, *Member, IEEE*, and Micky Rakotondrabe, *Member, IEEE*

SIMULATION RESULTS

For the simulation experiment, we chose the following system parameters: $\alpha_2 = 0.001[s]$, $\alpha_1 = 1$, $c_{ob} = 1[mNs/\mu m]$, $k_{ob} = 0.2675[mN/\mu m]$, $p = 1.3[\mu m/mN]$, $d_p = 1.0773[\mu m/V]$, $A_{bw} = 0.40648$, $B_{bw} = 0.40648$, and $\Gamma_{bw} = 0.00833$. The observer's parameters are $\theta = 8.8$, $k_o = 66.5945$, and $l_o = 10.2$. The control parameters are $k_1 = 120$, $k_2 = 100$, $M_1 = 7.1$, $L_1 = 7$, $M_2 = 16$, $L_2 = 15$, and $l = 0.65$. For the saturation function, we use a smooth function given by,

$$\sigma_i(s) = \begin{cases} \frac{\arctan(c_i[s-L_i])}{c_i} + L_i & \text{if } s > L_i \\ s & \text{if } |s| \leq L_i \\ \frac{\arctan(c_i[s+L_i])}{c_i} - L_i & \text{if } s < -L_i \end{cases} \quad (1)$$

where $c_i := \frac{\pi}{2(M_i - L_i)}$, with $M_i > L_i > 0$ for $i = \{1, 2\}$.

The system's initial conditions are $f(0) = 1.5[mN]$, $h(0) = 2$. While the initial conditions of the observer are all zero. The desired trajectory is given by [1],

$$\text{sqd}_c(t, \omega, \kappa) = \frac{\cos(\omega t)}{\sqrt{\kappa^2 \sin^2(\omega t) + \cos^2(\omega t)}} + 1; \quad (2)$$

with $\omega = 1$, $\kappa = 0.09$.

The force and hysteresis estimate with the proposed observer (19) are depicted in Fig. 1.

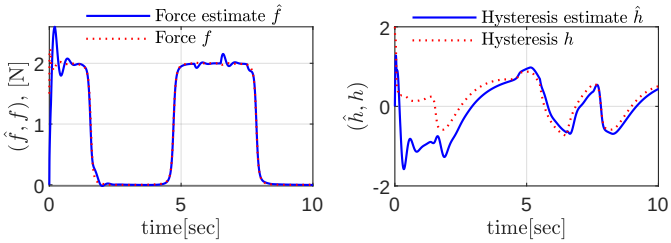

Fig. 1: Force and hysteresis estimates with the proposed observer. The convergence can be enhanced by conducting fine-tuning of the observer gains.

The force and its desired trajectory are depicted in Fig.2, where disturbance $\delta(t)$ is also shown. The disturbance is particularly severe at $t = 6$, but the controller's output feedback component can handle it effectively due to the accurate estimation of the disturbance.

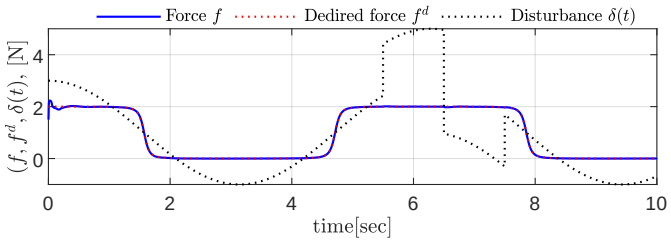

Fig. 2: The force f and the desired trajectory $f^d(t)$, and the disturbance $\delta(t)$. Notice how $\delta(t)$ is highly aggressive in $t \in [5.5, 6.5]$.

One of the primary objectives of control is to ensure that the tracking error remains within a predetermined set. This is demonstrated in Fig.3, where we can observe that the conditions of Assumption 4 are met. The error trajectory never exceeds the threshold marked in magenta at $l = 0.5$. By choosing appropriate initial conditions for the error and/or desired trajectory described in Assumption 4, we can further decrease this threshold.

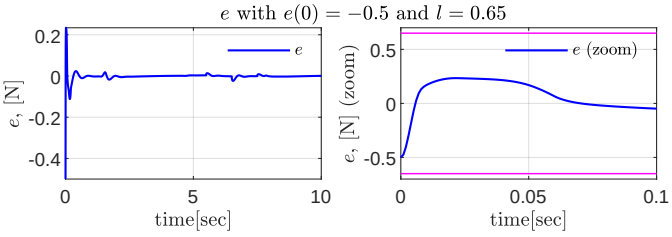

Fig. 3: The tracking error e and zoom of it. Notice that the e is always enclosed in the set $|e| < l$; the parameter l (and $-l$) appears magenta. The minor variations around $t = 6$ occur during the aggressive disturbance $\delta(t)$; please see Fig.2.

Fig.4 displays the proposed controller, the disturbance, and its estimate. Notably, the disturbance estimate initially exhibits an aggressive response, a normal occurrence due to the high-gain observer. The barrier term, represented by

$-\sigma_2\left(\frac{k_2 e}{l^2-e^2}\right)$, is responsible for aggressively rejecting any error that approaches l, whereas the proportional term, denoted by $-\sigma_1\left([l^2-e^2][k_1 e]\right)$, is more effective for errors near the origin. This is depicted in the example of Fig.5. Conversely, the smooth saturation functions $-\sigma_i(\cdot)$ serve the dual purpose of preventing spikes in the controller and allowing for the selection of high control gains. We have included a depiction of the argument of saturation functions $-\sigma_i(\cdot)$ in both cases, with and without saturation; see Fig.4. It is important to note that as the error term e approaches the value of l, the magnitude of the argument in the control term $-\sigma_2(\cdot)$ increases exponentially. Therefore, saturation functions become necessary to prevent this exponential response.

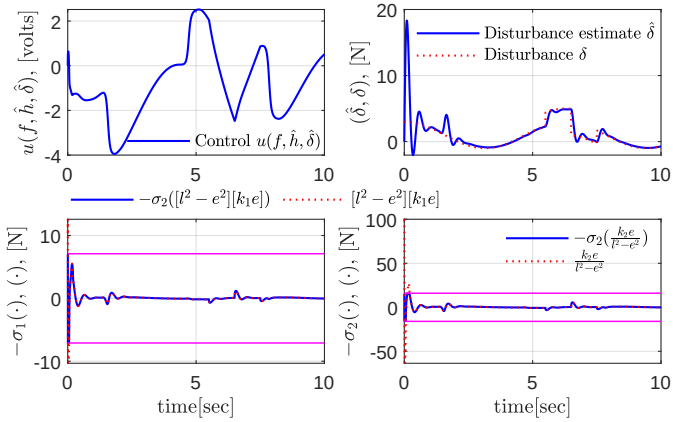

Fig. 4: Output feedback Barrier-Lyapunov-function and saturation-based controller, disturbance and its estimate, and the saturation terms of control (43). The saturation limits M_1 and M_2 are in magenta. To show the effect of the saturation control, we plot the arguments of saturation functions $-\sigma_1(\cdot)$ and $-\sigma_2(\cdot)$. Notice how the proposed control u maintains considerable limits and responds robustly against disturbances. This is due to the effect of saturation functions and the barrier term $k_2 e/(l^2-e^2)$.

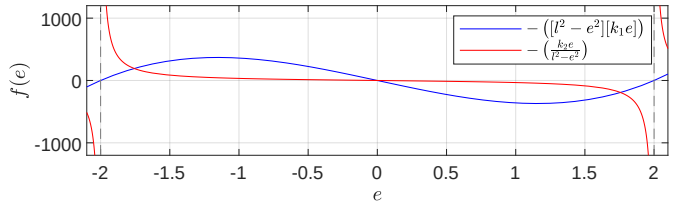

Fig. 5: This figure demonstrates the effectiveness of the proportional term (blue line) for errors close to the origin and the power of the barrier control term (red line) near the value of l, where, in this particular case, $l=2$.

The observer error convergence is depicted in Fig. 6. Notice that the high level of disturbance in the system causes some minor divergence in the observer error. The convergence rate can be improved by appropriately tuning the gains.

A. Simulation under parametric variations

In this section, we evaluate the performance of our control algorithm by subjecting it to various system parameters,

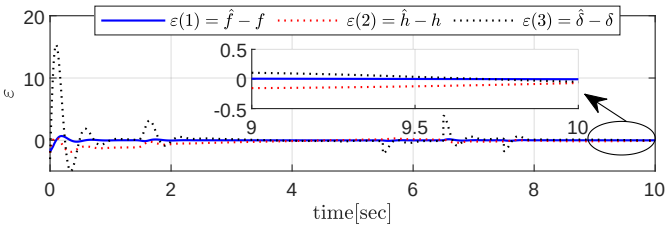

Fig. 6: This figure illustrates the effectiveness of the proposed observer, as evidenced by the convergence of observer errors to zero.

aiming to assess its robustness in different scenarios. We carefully select parameter sets that closely resemble real-world experimental conditions, ensuring the practicality and relevance of our investigation. Table I depicts the group of four parameters.

We simulate the closed-loop system with each of the four system parameter sets. To capture the performance of the closed-loop system, we conducted experiments without modifying any observer and control gains. In all four cases, we used the control gains described at the beginning of the first section of this supplementary material. Moreover, the system was subjected to the same initial conditions and external disturbances described above. The obtained results are visually presented in Figure 7. Notice that the convergence is practically the same with minimal variations in the transient response. This is due to the robustness capacity of our control to reject exogenous and aggressive disturbances maintaining the error enclosed in the set $(-l,l)$.

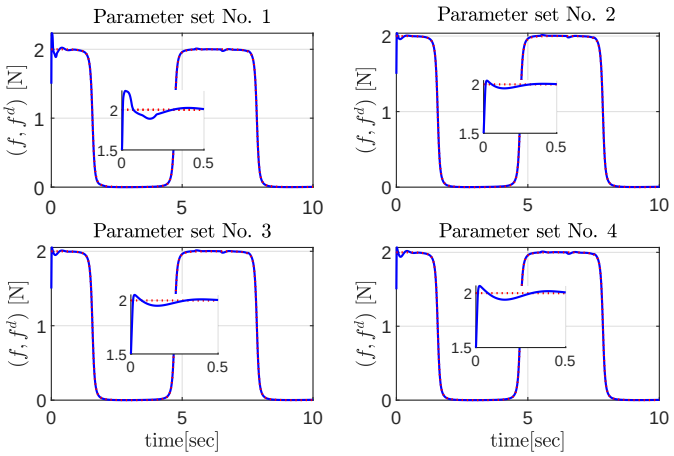

Fig. 7: Fig. The figure presented visually demonstrates the effectiveness of the proposed controller across four distinct sets of system parameters. In each case, the system is subjected to a disturbance $\delta(t)$ depicted in Fig. 2. The dotted red line represents the desired force f^d, while the solid blue line depicts the actual force. Notably, the control law exhibits an adept response regardless of the fluctuations in the system parameters.

TABLE I: Set of parameters used in the simulation.

Parameters set	α_1	α_2	d_p	ϱ	k_{ob}	c_{ob}	A_{bw}	B_{bw}	Γ_{bw}
Set No. 1	1	0.001	1.0773	1.3	1/3.738	1	0.40648	0.40648	0.00833
Set No. 2	1	0.001	1.11	1.8	1/1.5	1	0.11	0.00841	0.0084
Set No. 3	1	0.001	0.98	1.5	1/2	1	0.108	0.0079	0.0078
Set No. 4	1	0.001	1.0773	1.3	1/3.738	1	0.10648	0.00843	0.00833

B. Comparison with other controllers

In order to ensure a fair comparison with other controllers in the existing literature, it is crucial to have access to all system states, including the hysteresis h. However, due to the constraints specified in the problem statement, we can only utilize the feedback of f as per the given conditions. Nonetheless, to our knowledge, this is the first study that investigates the system in question using an output feedback scheme incorporating Barrier Lyapunov and saturation functions. Consequently, we employ our observer to incorporate the terms dependent on the hysteresis h in the comparative controllers discussed below. Our comparative analysis involves assessing the performance of the proposed control scheme against both a Proportional-Integral (PI) controller and a Sliding Mode Controller (SMC) with hysteresis feed-forward (FF) compensation. The PI controller with FF compensation is expressed as follows:

$$\dot{u}_{\text{PI}} = \frac{1}{a_2}\Big(-k_p e - k_i \int_{t_0}^{t} e\, d\tau + a_1 f - a_3 u + a_4 \dot{\hat{h}} + a_5 \hat{h}\Big). \quad (3)$$

where k_p and k_i are the proportional and integrative gains, respectively. The sliding mode controller with FF compensation is given by,

$$\begin{aligned} \dot{u}_{\text{SMC}} &= \frac{1}{a_2}\Big(-\bar{\beta}\,\text{sgn}\,(\sigma) + a_1 f - a_3 u + a_4 \dot{\hat{h}} + a_5 \hat{h}\Big) \\ \rho &= e + \bar{\alpha}\int_{t_0}^{t} e\, d\tau, \end{aligned} \quad (4)$$

where $\bar{\beta}$, $\bar{\alpha}$ are positive gains and ρ is the sliding surface.

For the simulation, we used the parameter set No.1 depicted in Table I. The control gains were meticulously tuned and selected: $k_p = 20$, $k_i = 1.3$, $\bar{\beta} = 12.5$, and $\bar{\alpha} = 8$. It is important to note that our controller's observer and control gains remain unchanged from the initial experiment. Additionally, to maintain consistency with the shape of the disturbance shown in Fig. 2, the external disturbance for this experiment has been deliberately set to three times the magnitude of the disturbance above. This is depicted in Fig. 8.

In this simulation experiment, we focus in the tracking error,

$$e = f - f^d. \quad (5)$$

For comparison, we compute its Euclidean norm together with its corresponding integral defined as,

$$\|e\| = \sqrt{e^2}, \quad \int_{t_o}^{t} \|e\| d\tau, \quad (6)$$

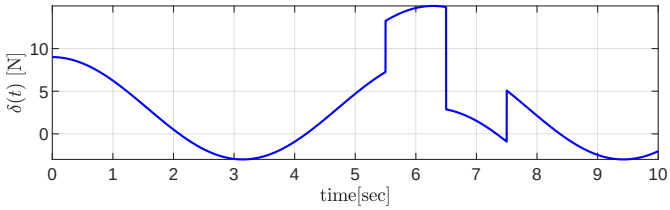

Fig. 8: The disturbance $\delta(t)$ used in the comparative study among PI+FF, SMC+FF, and our control.

respectively. The plots of these metrics for each controller are depicted in Fig. 9. The PI control and SMC with feedforward compensation are renowned for their robustness properties; however, they have certain limitations. Firstly, the PI+FF controller can effectively handle disturbances close to equilibrium. This is evident around $t = 6$ when the disturbance peak occurs. Secondly, the SMC+FF controller exhibits aggressive behavior, resulting in chattering in the system states and a high-frequency response in the control signal. This can be observed in the magnified view of the upper graph in Fig. 9, and it is an undesirable phenomenon for mechanical systems. In contrast, the proposed controller exhibits no chattering and demonstrates the capability to handle highly aggressive disturbances. Finally, the plots quantitatively show the efficiency of our approach among these robust controllers, even using our observer to estimate the hysteresis terms, as can be noted in (3), and (4).

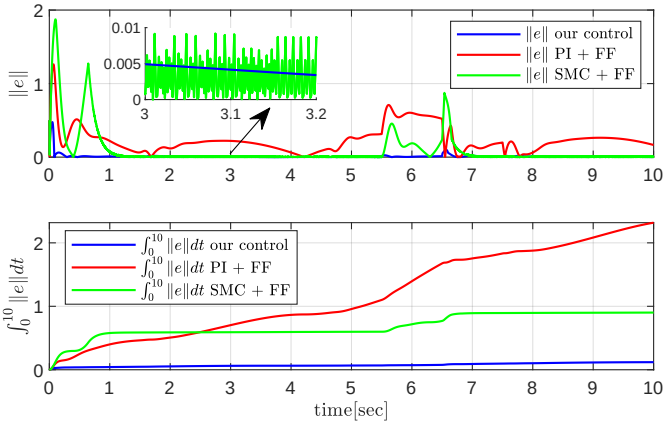

Fig. 9: Comparison of our controller versus the PID+FF and SMC+FF described in (3) and (4), respectively. We used the norm of the vector tracking error and its corresponding integral. Notice the undesirable chattering of the SMC+FF.

REFERENCES

[1] M. Fern-Guasti, "Squdel Function: Square Wave Approximation Without Ringing," *Circuits, Systems, and Signal Processing*, vol. 38, no. 2, pp. 764–773, Feb. 2019.